

Engineering Endochondral Bone: *In Vivo* Studies

Serafim M. Oliveira, M.S.,¹⁻⁴ Dindo Q. Mijares, D.D.S.,⁵ Gloria Turner, B.A.,⁴ Isabel F. Amaral, Ph.D.,¹ Mário A. Barbosa, Ph.D.,^{1,3} and Cristina C. Teixeira, D.M.D., M.S., Ph.D.^{4,5}

The use of biomaterials to replace lost bone has been a common practice for decades. More recently, the demands for bone repair and regeneration have pushed research into the use of cultured cells and growth factors in association with these materials. Here we report a novel approach to engineer new bone using a transient cartilage scaffold to induce endochondral ossification. Chondrocyte/chitosan scaffolds (both a transient cartilage scaffold—experimental—and a permanent cartilage scaffold—control) were prepared and implanted subcutaneously in nude mice. Bone formation was evaluated over a period of 5 months. Mineralization was assessed by Faxitron, micro computed tomography, backscatter electrons, and Fourier transform infrared spectroscopy analyses. Histological analysis provided further information on tissue changes in and around the implanted scaffolds. The deposition of ectopic bone was detected in the surface of the experimental implants as early as 1 month after implantation. After 3 months, bone trabeculae and bone marrow cavities were formed inside the scaffolds. The bone deposited was similar to the bone of the mice vertebra. Interestingly, no bone formation was observed in control implants. In conclusion, an engineered transient cartilage template carries all the signals necessary to induce endochondral bone formation *in vivo*.

Introduction

WITH INCREASING TIME of life expectation, the economic impact of musculoskeletal diseases may now exceed 2.5% of the Gross National Product in the United States.¹ Among these diseases, problems related to bone loss are one of the major causes of disability. To replace lost bone, surgeons use autografts, considered the ideal grafting material. This approach presents disadvantages such as donor site morbidity and limited supply, which in most of cases is insufficient.² Due to these limitations, it is imperative to find new alternatives to autografts. Allografts and xenografts are reasonable substitutes, but they also have serious limitations like the risk of rejection or disease transmission. To overcome these shortcomings, several bone grafting materials have been engineered, including ceramics, metals, synthetic, and natural polymers. In most cases, materials are implanted into surgically created bone defects, and new bone grows on their surfaces and within their matrices. Under these conditions, it is believed that the bone is formed by osteoblasts that migrated from the adjacent original bone and marrow cavities, a mechanism that is referred to as osteoconduction. Although this osteointegration is important and essential, there are situations (e.g., large defects) where the scaffolds, besides pro-

viding the template for tissue regeneration, need to be osteoinductive, that is, stimulate the migration of undifferentiated cells and induce their differentiation into active osteoblasts in order to promote *de novo* bone formation. To improve the osteoinductive properties of grafting materials, they have been combined with growth factors and different cells types with variable results depending on the host regenerative capability.^{3,4} Therefore, osteoinductive approaches are crucial when the bone regenerative ability is diminished or lost. Here we propose a novel approach in bone tissue engineering and the creation of an improved osteoinductive material for bone regeneration.

In the body, cartilaginous tissues can be divided into permanent and transient. While having the same embryonic origin, permanent and transient cartilages follow distinct differentiation pathways, fulfill different functions, and ultimately as their names suggest have different fates. Articular, tracheal, and other cartilage structures are classified as permanent cartilage. The chondrocytes in these structures maintain a relatively stable phenotype and persist for many years.⁵ In contrast, most of the embryonic cartilaginous skeleton, the epiphyseal growth plates of long bones, the cartilaginous callus formed at fracture sites, and the tissue created during distraction osteogenesis consist of transient cartilage.^{6,7} This

¹Department of Mechanical Engineering, ESTV—Escola Superior de Tecnologia de Viseu, Viseu, Portugal.

²Divisão de Biomateriais, INEB—Instituto de Engenharia Biomédica, Porto, Portugal.

³FEUP—Faculdade de Engenharia da Universidade do Porto, Department of Metallurgy and Materials, Porto, Portugal.

⁴Department of Basic Science and Craniofacial Biology, New York University College of Dentistry, New York, New York.

⁵Department of Biomaterials and Biomimetics, New York University College of Dentistry, New York, New York.

transient cartilage is gradually replaced by bone through a series of maturational changes during the process of endochondral bone formation. Indeed, this is the mechanism responsible for formation of most of our skeleton, and for postnatal growth.

Surprisingly, except for few reports, the bone tissue engineering field has focused on generating bone directly from osteoprogenitor cells or osteoblasts. Montufar-Solis *et al.*⁸ prepared aggregates of mouse embryonic limb cells that after implantation in mice induced endochondral bone formation. Indeed, the endochondral pathway for bone formation can be activated using biomaterials carrying mesenchymal stem cells,⁹ bone morphogenetic proteins (BMPs),¹⁰ or plasmid DNA encoding for BMPs.^{11,12} To date, only Alsberg *et al.*¹³ deliberately explored the endochondral pathway by implanting in mice, articular chondrocytes mixed with calvarial osteoblasts using an alginate carrier. *In vivo*, the tissue organized in a manner similar to a growth plate. This effect is not totally surprising if one considers that hypertrophic chondrocytes secrete factors capable of inducing vascularization, osteoblast, and osteoclast activity.¹⁴⁻¹⁷ The interplay of these different cell types is required for endochondral bone formation. Therefore, in the current work, we created a transient cartilage scaffold as a template for *in vivo* endochondral ossification. We tested the hypothesis that this transient cartilage, as an osteoinductive scaffold, carries all the signals necessary to induce new bone formation once implanted *in vivo*, even subcutaneously.

Materials and Methods

In vitro studies

Transient cartilage scaffolds. The chondrocyte/chitosan scaffolds used in this work were characterized extensively (see accompanying article).¹⁸ Briefly, chitosan sponges were prepared from a 2% (w/v) chitosan solution by a freeze/drying process and then cut into small pieces (4×4×1 mm³). Cephalic (CP) and caudal (CD) chondrocytes isolated from the upper and lower regions of sternum of 14th-day chicken embryos were allowed to proliferate in 100-mm dishes for 7 days in Dulbecco's modified high-glucose Eagle's medium (DMEM) containing 10% NU Serum and 100 U/mL of penicillin/streptomycin (Fisher Scientific, Fairlawn, NJ), before being seeded into the chitosan sponges and cultured for 20 days at 37°C and 5% CO₂ in the same conditions. During the last 10 days, cultures were treated with 100 nM all-trans retinoic acid (RA) in order to induce chondrocyte maturation and matrix deposition. Prior to implantation, at day 20, alkaline phosphatase (AP) activity and protein content were measured following the protocols described by the accompanying article,¹⁸ to confirm maturation.

In vivo studies

Surgical procedures. Adult male athymic NCr-nu/nu mice (Charles River Laboratories, NY) were used as surgical recipients. The animal experiments were conducted according to the guidelines of the Institutional Animal Care and Use Committee (IACUC) of New York University. Briefly, mice were received 1 week before scheduled surgery and fed a regular diet and sterile water, ad libitum. After surgery and for

1 week, trimethoprim and sulfamethoxazole (20 and 100 mg/L, respectively) were added to sterile drinking water. Surgeries were performed under strict aseptic and warm conditions, with general anesthesia produced by intraperitoneal injection of ketamine (80 mg/kg) and xylazine (10 mg/kg). Lateral longitudinal skin incisions were made in both sides of the mice dorsum, and a subcutaneous pocket (1 to 1.5 cm) was created for implantation of the chondrocyte/chitosan scaffolds. On the right side, we implanted the scaffolds seeded with CP chondrocytes (experimental implant), whereas the left side received the scaffolds seeded with CD chondrocytes (control). Incisions were closed with surgical staples. Two or three sponges were implanted on each side. Results shown represent three independent experiments, different surgeries, using three independent groups of implants (i.e., sponges hydrated in different periods, primary cells harvested from different chicken embryos, and mice received at different times). In the first experiment, 11 mice received implants; in the second and third experiments, 14 and 22 mice were implanted, respectively. All animals, except three mice that did not recover from anesthesia, survived the surgical procedures.

Euthanasia and sample collection. The mice were sacrificed at 1, 2, 3, 4, and 5 months postoperatively, and implants and surrounding tissues harvested. Briefly, animals were exposed to a gas mixture of 30% of CO₂ and 70% of O₂ for 1 min followed by CO₂ 100% during 4 min until no signal of breathing was detected. Tissue/samples were collected and immediately immersed in 10% phosphate buffer formalin for future analysis.

Faxitron and micro computed tomography. All fixed tissues were radiographed in a high-resolution X-ray machine (Faxitron Series 43805N; Hewlett Packard, McMinnville, OR) set at 25 kVp, and 2.5 mA for 15 s, using a KODAK dental film (Kodak, Rochester, NY). Films were developed and scanned on a Gendex GXP dental X-ray processor (Gendex, Lake Zurich, IL) and on a Minolta Dimage Scan Dual II (Konica, New York, NY), respectively. The same samples were scanned by micro computed tomography (microCT, μ CT40; Scanco Medical, Basserdorf, Switzerland). Wet fixed tissues were placed in the microCT specimen holder, and sealed to prevent tissues from drying. Scans were performed using high resolution (10 μ m nominal resolution) to assess the new mineralized structure formed. Data were collected at 55 kVp and 145 μ A, and reconstructed applying the cone-beam algorithm supplied by Scanco Medical. For visualization and three-dimensional (3D) evaluation, images were filtered using a constrained 3D Gaussian filter to partially suppress noise in the volumes ($\sigma = 1.2$ and support = 1), and binarized using a threshold in the range 255 to 1000. The minimum threshold value was calculated comparing the two-dimensional reconstructed images from our scans to images obtained from μ CT Evaluation Program V5.0. In addition, we performed CT-based morphometric analyses of bone volume/total volume (BV/TV).

Scanning electronic microscopy. For scanning electronic microscopy (SEM) analysis, fixed samples were dehydrated in

an ethanol series and critical-point dried. Samples were then cut, glued on steel stubs, coated with carbon, and analyzed on cross-sectional areas using SEM. Images of mineral phases were obtained from backscatter electrons (BSE), and its chemical composition was determined by energy-dispersive X-ray microanalysis (EDAX).

Fourier transform infrared spectroscopy. For Fourier transform infrared spectroscopy (FTIR), samples were reduced to powder and analyzed as KBr pellets using a Nicolet-Magna 550 FTIR Series-II spectrometer (GMI, Ramsey, MN). Analyses were performed in implanted materials as well as in mouse original bone (vertebras) for comparison. Before preparation of pellets, implants were dried in an oven overnight.

Histology evaluation. Implants were collected and fixed in 10% phosphate buffer formalin, demineralized for 15 days, dehydrated in alcohol series, embedded in paraffin, and 5- μ m-thick sections cut using a microtome. Sections were mounted on glass slides, stained with hematoxylin and eosin (H&E), and scanned on Scan Scope GL series optical microscope (Aperio, Bristol, UK).

Statistical analysis. All experiments were repeated three to four times, and the mean and standard error of the mean were determined. Significant differences were assessed by ANOVA. A *p*-value refers to a comparison of a measured parameter in the experimental group with that of the appropriate control; significance was set at $p < 0.05$.

Results

Overview of experimental procedure

Figure 1 shows a schematic of the experimental approach in this study. Images (SEM) of chitosan sponges, a mouse, and an X-ray image of the implanted area 3 months after implantation are displayed. The implant on the right side (CP chondrocytes) reveals the ability of those cells to mineralize, and the similarity between its density and the mouse bone density can be observed. In contrast, the implant on the left side did not mineralize; therefore, no radiopaque area can be observed.

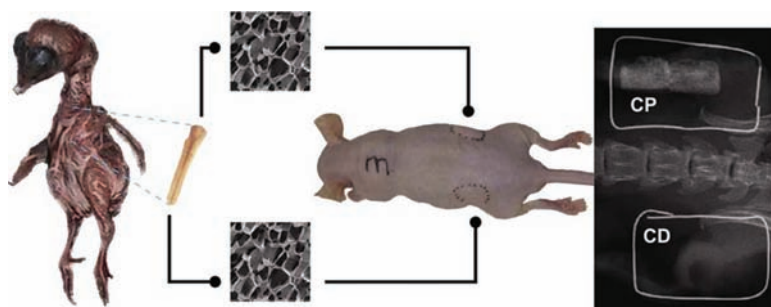


Figure 1 shows a schematic of the experimental approach in this study. Images (SEM) of chitosan sponges, a mouse, and an X-ray image of the implanted area 3 months after implantation are displayed. The implant on the right side (CP chondrocytes) reveals the ability of those cells to mineralize, and the similarity between its density and the mouse bone density can be observed. In contrast, the implant on the left side did not mineralize; therefore, no radiopaque area can be observed.

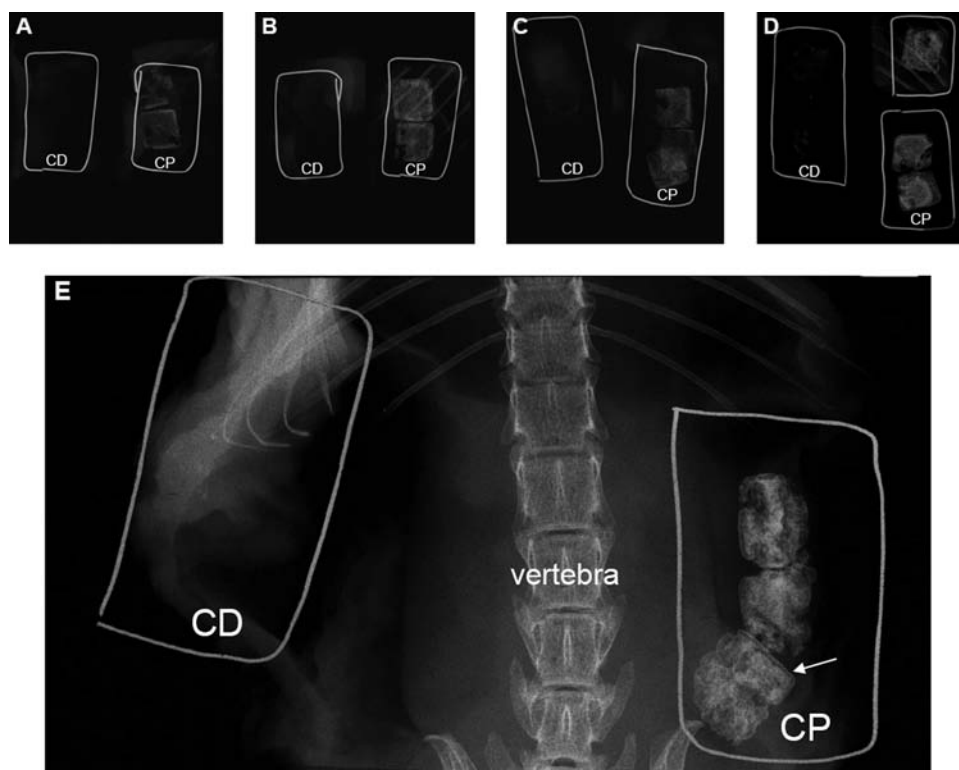
Mineral distribution in the implants

In vivo studies were conducted for 5 months, and mice were collected for analysis every month. Mineralization of experimental implants (scaffolds seeded with CP chondrocytes) was achieved in all scaffolds as confirmed by fine-focus radiographs. As early as 1 month after implantation, an increase in density was observed on the periphery of the experimental implants (Fig. 2A—CP), which is attributable to the presence of mineral. From the second to the fifth month postimplantation (Fig. 2B—CP to 2E—CP, respectively), the amount of mineral increased gradually. In Figure 2B and D, implants can be observed in the vicinity of the mouse ribs showing similar radiopacity to the mouse bones. In the fifth month after implantation (Fig. 2E—CP), radiographs of implants and the mouse skeleton allow comparison between the vertebra and the scaffolds indicating considerable bone/mineral deposition in response to CP chondrocyte signaling. In addition, a thin “cortical layer” is observed (Fig. 2E, white arrow) on the periphery of the implants. For all the time points studied, no comparable radiopacity was observed on control implants (images marked with CD); the density of these implants is similar to the soft tissue in the absence of mineralization.

Mineral distribution across the experimental implants was assessed by microCT scans as shown in Figure 3. MicroCT results confirm that 1 month after implantation, mineralization has occurred only in limited areas at the surface (Fig. 3A) of the experimental implants. Two months after implantation (Fig. 3B), mineral can be found in almost all areas of the implant with a homogeneous distribution. On the third (Fig. 3C) and fourth (Fig. 3D) months after implantation, the mineral becomes denser and only few areas remain unmineralized. In the fifth month postimplantation (Fig. 3E), the mineral density is significantly increased on the surface as well as inside of the implant, as observed in the cross-sectional image (Fig. 3F). As in the Faxitron images, a layer of mineral can be observed on all the surface of the scaffold, suggesting the formation of a cortical bone-like structure. Deeper into the scaffold, mineral is observed both in cartilage as well as in areas of bone formation (compare with histology images). Mineral quantification using microCT scans (Fig. 3G) confirms a time-dependent increase (more than 10-fold) in mineral volume during the implantation period studied. Control implants (CD chondrocytes) were also analyzed by microCT; however, at the threshold used for data processing, only a few speckles of mineral were observed (data not shown).

FIG. 1. Schematic of experimental design. CP and CD chondrocytes were removed from the sterna of chick embryos and seeded into chitosan sponges. After treatment with RA to induce chondrocyte maturation, chondrocyte/chitosan scaffolds were implanted into subcutaneous pouches on each side of the vertebral column of nude mice. Mice were euthanized (at least five mice each month for 5 months after implantation), and different analyses performed to evaluate bone formation. The whole mouse radiographic image shows mineraliza-

FIG. 2. High-resolution radiography shows an increase in mineralization during the implantation period. Samples were collected every month, for 5 months after implantation, and radiographed by Faxitron (25 kV/15 s). Radiographic images (A) to (E) correspond to scaffolds implanted from 1 to 5 months, respectively (A = 1 month, B = 2 months, C = 3 months, D = 4 months, and E = 5 months). On the left side of each photomicrograph, inside wire "boxes," are scaffolds cultured with CD chondrocytes, and on the right side, scaffolds cultured with CP chondrocytes (same mouse). Wires were used to help localize the scaffolds, especially in the absence of mineralization. Image (E) shows mouse vertebral bodies and ribs as well as a thin mineralized layer (arrow/CP sample) similar to cortical bone.



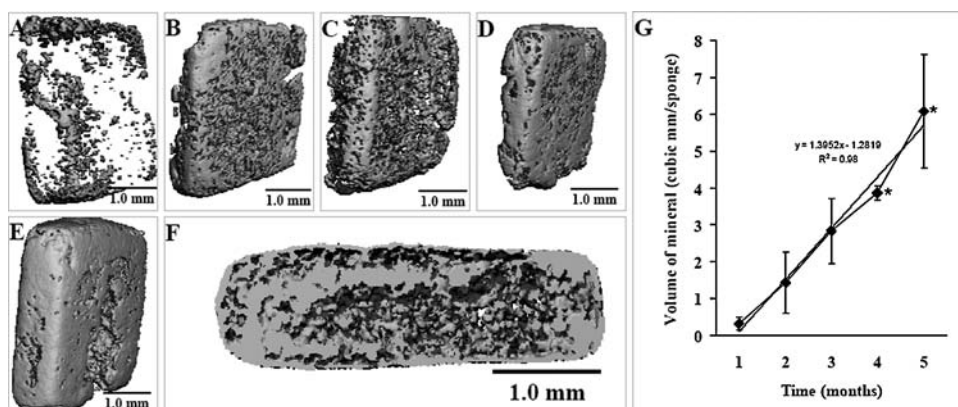
Characterization of the composition and structure of the mineral

The BSE results identified a thin layer of mineral on the surface of the experimental implants (Fig. 4C) and show that the mineralization occurred across the implant. On control implants (Fig. 4B), minimal mineralization has occurred. The quantitative analyses performed using EDAX allowed us to identify Ca and P (Fig. 4D) as the main elements present in the

mineralized regions (white areas) of the experimental implants, whereas in control (Fig. 4A) only C and O elements were detected.

In Figure 5 we compared the FTIR spectra of bone from vertebra of the mouse, with the experimental and control implants. FTIR spectrum of material collected from vertebra revealed the characteristic peaks corresponding to the mineral phase of the bone as well as peaks corresponding to the organic phase. In the mineral phase, peaks represent carbonate

FIG. 3. Accumulation of mineral in experimental scaffolds during the implantation period. Images obtained from microCT scans (3D) show gradual accumulation of mineral in the experimental scaffolds (CP chondrocytes) during the 5 months of implantation. Images (A) to (E) correspond to samples collected from month 1 to month 5, respectively, and image (F) is the cross section of (E) (month 5). An increase of dense material is observed over time. After 5 months of implantation, mineralization is observed across the chondrocyte/chitosan scaffold (F). At the threshold used to collect these data, no mineral was observed in the control implants (CD chondrocytes, not shown). Volume of mineral was calculated from microCT scans and graphed as mean \pm SD (panel G). At least five sponges were used to calculate the volume of mineral for each time point. Asterisk (*): Significantly different from previous months ($p < 0.05$).



After 5 months of implantation, mineralization is observed across the chondrocyte/chitosan scaffold (F). At the threshold used to collect these data, no mineral was observed in the control implants (CD chondrocytes, not shown). Volume of mineral was calculated from microCT scans and graphed as mean \pm SD (panel G). At least five sponges were used to calculate the volume of mineral for each time point. Asterisk (*): Significantly different from previous months ($p < 0.05$).

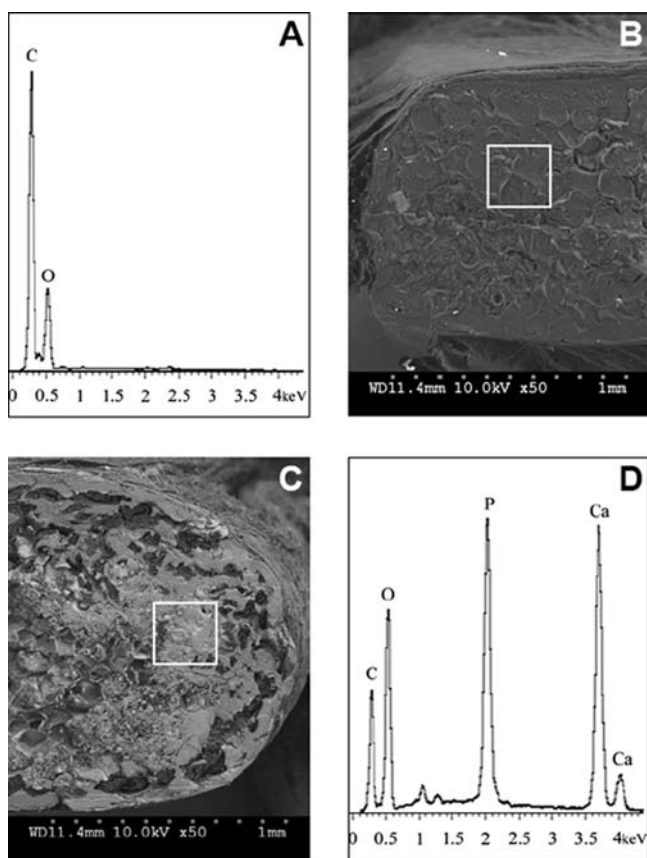


FIG. 4. Backscattering SEM and chemical composition after 5 months of implantation. Photomicrographs were obtained from BSE in a scanning electron microscope, and they show cross sections of control implant (**B**) and the experimental implant (**C**). White areas represent the mineralized regions, and gray areas correspond to soft tissue. Qualitative analysis was determined using SEM/EDAX (**A**, **D**). In the middle of experimental implant, we observed an area rich in Ca and P, while in control implant only C and O can be detected. Note the presence of bone-like layer similar to cortical bone on the surface of experimental implant (**C**), and the larger thickness of the experimental implant suggesting growth.

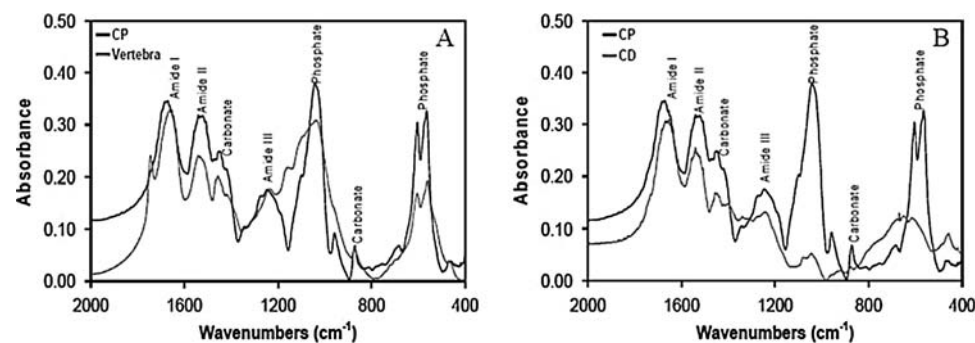


FIG. 5. FTIR analyses of mouse vertebra, experimental and control scaffolds. Samples were dissected at the end of 5 months of implantation, dried, and mixed with KBr to prepare pellets for FTIR analyses. (**A**) Spectra of mouse vertebral bone and experimental (CP chondrocytes) scaffold both showing the presence of absorbance bands for phosphate and carbonate. (**B**) In the control (CD chondrocytes) scaffold, the absorbance bands for phosphate and carbonate are much lower than that in experimental scaffold.

(CO₃) and phosphate (PO₄) groups. The experimental implants (CP) showed a very similar spectrum. In the control implants (CD), these peaks were not observed.

Histology

Histological sections stained with H&E (Fig. 6) reveal the tissue changes that occurred during the implantation period. Figure 6A–D shows details of the experimental samples during the first 4 months of implantation. A bone-like layer (arrows) formed at the surface of the scaffold as early as 1 month after implantation, while 3 and 4 months after implantation, we can observe the formation of bone marrow-like structures (Fig. 6C, D). The vascular invasion of the cartilage matrix is also observed as earlier as 1 month (arrow head in Fig. 6E). In the following months (Fig. 6F–H), vascular invasion continues deep into the sponges, and bone is deposited around these channels. In Figure 6I (a complete section through the mouse body), we can observe the implants as well as the vertebral bone. In the control implant (left side), only cartilage tissue can be seen. In the experimental implant (right side), a cortical layer of bone has formed, strikingly very similar in thickness to the cortical bone in the vertebral bodies (compare Fig. 6K with 6L). Further, bone is forming across the experimental implant, along with bone marrow cavities, while in the control (Fig. 6J, M, and P), mostly chondrocytes and fibrous tissue can be seen invading the scaffold. At high magnification and deep into the sponges (Fig. 6O, arrow heads), we can observe both vascular invasion of chondrocytes and bone deposition, consistent with changes observed at the chondroosseous junction in growth plates.

Discussion

Our *in vitro* studies demonstrated that a 3D chitosan sponge can support chondrocyte proliferation and hypertrophy, characterized by expression of type X collagen and high AP activity (see accompanying article).¹⁸ To test the hypothesis that such a transient cartilage template carries all the signals necessary to induce new bone formation, we implanted these cartilage/chitosan scaffolds into the subcutaneous region of nude mice and evaluated mineralization and new bone formation over a period of 5 months. As control, we used sponges seeded with CD sternal chondrocytes, shown to maintain a permanent cartilage phenotype after treatment with RA.

FIG. 5. FTIR analyses of mouse vertebra, experimental and control scaffolds. Samples were dissected at the end of 5 months of implantation, dried, and mixed with KBr to prepare pellets for FTIR analyses. (**A**) Spectra of mouse vertebral bone and experimental (CP chondrocytes) scaffold both showing the presence of

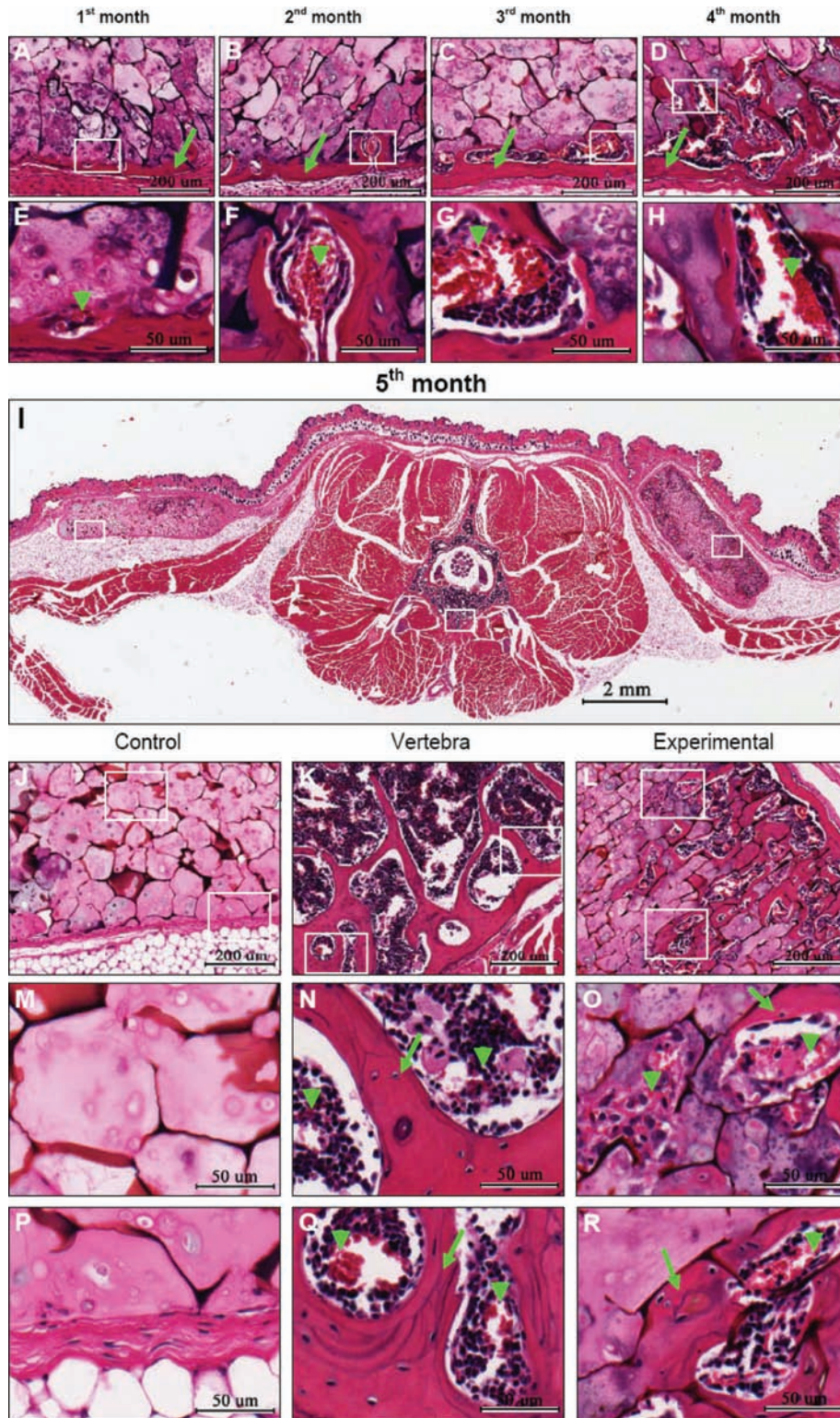


FIG. 6. Histological analysis of chondrocyte/chitosan scaffolds implanted in the subcutaneous region of nude mice. Axial paraffin sections were cut through the body of the mouse (E) to include the experimental and control scaffolds. Sections were stained with H&E and photographed. Details of bone forming in experimental scaffolds during the first 4 months of implantation are shown in images (A) through (D). Images (E), (F), (G), and (H) correspond to high magnifications of (A), (B), (C), and (D), respectively, showing the beginning of vascular invasion (arrow heads). The control scaffolds do not undergo visible changes during the first 5 months of implantation, and therefore only the fifth month is included in this figure. A complete section is shown after 5 months of implantation in image (I). Control scaffold is on the left and experimental is seen on the right side of the image. Details of control scaffold (J), vertebral body (K), and experimental scaffold (L) can be observed. Higher magnifications of control (M, P), mouse vertebra (N, Q), and experimental scaffold (O, R) show tissue details. Deep in the control sample (M), only cartilage tissue can be observed. Vascular invasion of cartilage (arrow head in O) and bone deposition (arrow in O) can be observed in the experimental sample. Detail of vertebra (N, Q) shows the presence of bone (arrow) and blood vessels (arrow head). Note bone formation deep in the experimental scaffold as well as the presence of blood vessels (R). Color images available online at www.liebertonline.com/ten.

A plethora of studies have successfully induced new bone formation after implantation of different materials in areas adjacent to or in holes drilled into bone structures of animals.^{3,4,19–21} Others have implanted materials subcutaneously or intramuscularly, and used stem cells, bone differentiation factors, or gene therapy to enhance new bone formation at these ectopic areas.^{22,23} In addition, it was shown that combining human bone marrow stromal cells, fibroblasts, and primary articular chondrocytes could result in ectopic bone formation.^{12,24–26} On the other hand, most of the studies using chondrocytes focus on articular cartilage reconstruction^{27–31} or implanted the cartilage in bone-forming areas.^{8,32} However, in our investigation we choose to implant the cartilage/chitosan scaffolds into a non-bone-forming area (subcutaneous regions) to investigate the osteoinductive potential of hypertrophic chondrocytes without the use of any bone differentiation factor or gene therapy. Indeed, as soon as 1 month after implantation, mineral deposition was observed by microCT and Faxitron analyses. These scaffolds were not mineralized *in vitro*, for a variety of reasons discussed in the accompanying manuscript.¹⁸ However, *in vivo*, and as expected, hypertrophic chondrocytes with high AP activity in a matrix rich in type X collagen rapidly triggered the mineralization phenomenon throughout the scaffold.^{33–36} The main peaks in the EDAX spectrum showed the presence of Ca and P in these scaffolds, major components of mineral both in bone and growth cartilage.^{37,38} The FTIR spectrum of the mineral formed in the CP constructs is identical to that obtained from the mouse vertebra, and the spectra described in the literature for bone.^{39,40}

Interestingly, microCT, BSE, and histological analyses revealed the formation of a cortical layer of bone on the surface of the experimental scaffolds^{20,32} as early as 1 month after implantation. The presence of osteocyte-like cells in that layer was confirmed in the H&E-stained sections. Other studies have shown that the bone structure formed in response to signals generated by the hypertrophic chondrocytes resembles the metaphyseal cortical bone⁴¹ formed during endochondral ossification. Indeed, in our experimental scaffolds, we observed phenotypical changes and tissue transformations that closely recapitulate the activity of the cells in the growth plate and at the chondroosseous junction during endochondral bone formation. Chondrocyte hypertrophy was induced *in vitro* (see accompanying article),¹⁸ while mineralization of the cartilage matrix occurred after implantation, *in vivo*. The experimental scaffolds also induced abundant vascularization and extensive bone deposition, even in areas located deep into the scaffold. Further, the bone deposited in our experimental scaffolds shows striking similarities (in the thickness of the cortical plate, the size of the marrow cavities, and trabeculae forming deep into the scaffold) to the endochondral bone of the mouse vertebra.

Interestingly, over the period of 5 months, the experimental cartilage/chitosan scaffold and the bone forming in and around it increased in size as can clearly be observed when comparing control and experimental BSE images. This is not totally unexpected, since during endochondral ossification, there is interstitial growth resulting from proliferation, hypertrophy, and *de novo* bone deposition. All those processes are at play in our attempt to engineer endochondral bone. While the scaffolds in the current implantation sites were not subject to compressive forces (possibly stretching through the

skin), evidence suggest that introducing mechanical stimuli in future approaches will allow us to direct the bone growth process.^{42–44}

Other interesting questions warrant a detailed investigation. Since the instructions for bone formation by our mammalian host originated from avian chondrocytes, we are curious about the nature of the bone tissue deposited in these scaffolds. Does the bone formed resemble mammalian or avian bone? In addition, and as some researchers proposed,³³ can chick chondrocytes transdifferentiate into “bone like cells” depositing the first layers of bone? Another question relates to the stability of the bone formed. Will endochondral ossification proceed beyond 5–6 months of implantation and will we observe further increase in the size of the original scaffold? Current and future studies in our laboratory will attempt to address these issues.

Conclusion

We have presented evidence that a transient cartilage scaffold (CP chondrocytes) created *in vitro* carries all the signals necessary to induce ectopic new bone formation *in vivo*, while a permanent cartilage scaffold failed to do so (CD chondrocytes). We extended our study beyond the 2 months of observation that characterize most bone tissue engineering approaches,^{20,23,32,45} to study the stability of the bone formed and its potential to grow. We are very excited to report that endochondral ossification (subcutaneously) proceeded in a manner strikingly similar to the endochondral ossification occurring in the vertebra of the host, the mice. The nature of the bone formed in response to the chick cartilage signals, the amount, and the increase in bone tissue over the first year of implantation are currently under investigation in our laboratory. We believe that this represents an optimized approach to bone grafting of large defects and in growing patients. The source of chondrocytes for such a clinical application would be autologous cartilage from the host (nasal, ear, or costochondral) or chondrocytes obtained from different stem cell sources that could be induced to hypertrophy *in vitro* before implantation. A very promising approach is the use of autologous chondrocytes obtained from a bioreactor created in the space under the periosteum of the host.⁴⁶ Given that chitosan in different formulations and for multiple applications (health and food industry) is currently FDA approved,⁴⁷ we do not anticipate major obstacles to its use in humans for the novel bone regeneration approach we propose in these studies.

Acknowledgments

This work was supported by the Luso-American Development Foundation (Portugal), the Calouste Gulbenkian Foundation (Portugal), PRODEP (Portugal), the American Association of Orthodontics Foundation, and NIDCR grant 5K08DE017426. The authors would like to thank Mr. Nuno Pontes for the illustration work.

References

1. Yelin, E., and Callahan, L.F. The economic cost and social and psychological impact of musculoskeletal conditions. National Arthritis Data Work Groups. *Arthritis Rheum* 38, 1351, 1995.

2. Service, R.F. Tissue engineers build new bone. *Science* **289**, 1498, 2000.
3. Dupraz, A., Delecrin, J., Moreau, A., Pilet, P., and Passuti, N. Long-term bone response to particulate injectable ceramic. *J Biomed Mater Res* **42**, 368, 1998.
4. Gauthier, O., Khairoun, I., Bosco, J., Obadia, L., Bourges, X., Rau, C., Magne, D., Bouler, J.M., Aguado, E., and Daculsi, G. Noninvasive bone replacement with a new injectable calcium phosphate biomaterial. *J Biomed Mater Res* **66A**, 47, 2003.
5. Maroudas, A., Bayliss, M.T., Uchitel-Kaushansky, N., Schneiderman, R., and Gilav, E. Aggrecan turnover in human articular cartilage: use of aspartic acid racemization as a marker of molecular age. *Arch Biochem Biophys* **350**, 61, 1998.
6. Ferguson, C., Alpern, E., Miclau, T., and Helms, J.A. Does adult fracture repair recapitulate embryonic skeletal formation? *Mech Dev* **87**, 57, 1999.
7. Iwamoto, M., Higuchi, Y., Enomoto-Iwamoto, M., Kurisu, K., Koyama, E., Yeh, H., Rosenbloom, J., and Pacifici, M. The role of ERG (ets related gene) in cartilage development. *Osteoarthritis Cartil* **9 Suppl A**, S41, 2001.
8. Montufar-Solis, D., Nguyen, H.C., Nguyen, H.D., Horn, W.N., Cody, D.D., and Duke, P.J. Using cartilage to repair bone: an alternative approach in tissue engineering. *Ann Biomed Eng* **32**, 504, 2004.
9. Pountos, I., Jones, E., Tziouppis, C., McGonagle, D., and Giannoudis, P.V. Growing bone and cartilage: the role of mesenchymal stem cells. *J Bone Joint Surg Br* **88**, 421, 2006.
10. Valimaki, V.V., Yrjans, J.J., Vuorio, E.I., and Aro, H.T. Molecular biological evaluation of bioactive glass microspheres and adjunct bone morphogenetic protein 2 gene transfer in the enhancement of new bone formation. *Tissue Eng* **11**, 387, 2005.
11. Huang, Y.C., Simmons, C., Kaigler, D., Rice, K.G., and Mooney, D.J. Bone regeneration in a rat cranial defect with delivery of PEI-condensed plasmid DNA encoding for bone morphogenetic protein-4 (BMP-4). *Gene Ther* **12**, 418, 2005.
12. Bikram, M., Fouletier-Dilling, C., Hipp, J.A., Gannon, F., Davis, A.R., Olmsted-Davis, E.A., and West, J.L. Endochondral bone formation from hydrogel carriers loaded with BMP2-transduced cells. *Ann Biomed Eng* **35**, 796, 2007.
13. Alsberg, E., Anderson, K.W., Albeiruti, A., Rowley, J.A., and Mooney, D.J. Engineering growing tissues. *Proc Natl Acad Sci USA* **99**, 12025, 2002.
14. Deckers, M.M., Karperien, M., van der Bent, C., Yamashita, T., Papapoulos, S.E., and Lowik, C.W. Expression of vascular endothelial growth factors and their receptors during osteoblast differentiation. *Endocrinology* **141**, 1667, 2000.
15. Petersen, W., Tsokos, M., and Pufe, T. Expression of VEGF121 and VEGF165 in hypertrophic chondrocytes of the human growth plate and epiphyseal cartilage. *J Anat* **201**, 153, 2002.
16. Nakagawa, M., Kaneda, T., Arakawa, T., Morita, S., Sato, T., Yomada, T., Hanada, K., Kumegawa, M., and Hakeda, Y. Vascular endothelial growth factor (VEGF) directly enhances osteoclastic bone resorption and survival of mature osteoclasts. *FEBS Lett* **473**, 161, 2000.
17. Gerber, H.P., Vu, T.H., Ryan, A.M., Kowalski, J., Werb, Z., and Ferrara, N. VEGF couples hypertrophic cartilage remodeling, ossification and angiogenesis during endochondral bone formation. *Nat Med* **5**, 623, 1999.
18. Oliveira, S.M., Amaral, I.F., Barbosa, M.A., and Teixeira, C.C. Engineering endochondral bone: *in vitro* studies. 2007.
19. Hasegawa, S., Ishii, S., Tamura, J., Furukawa, T., Neo, M., Matsusue, Y., Shikinami, Y., Okuno, M., and Nakamura, T. A 5–7 year *in vivo* study of high-strength hydroxyapatite/poly(L-lactide) composite rods for the internal fixation of bone fractures. *Biomaterials* **27**, 1327, 2006.
20. Gauthier, O., Muller, R., von Stechow, D., Lamy, B., Weiss, P., Bouler, J.M., Aguado, E., and Daculsi, G. *In vivo* bone regeneration with injectable calcium phosphate biomaterial: a three-dimensional micro-computed tomographic, biomechanical and SEM study. *Biomaterials* **26**, 5444, 2005.
21. Chan, C., Thompson, I., Robinson, P., Wilson, J., and Hench, L. Evaluation of Bioglass/dextran composite as a bone graft substitute. *Int J Oral Maxillofac Surg* **31**, 73, 2002.
22. Trojani, C., Boukhechba, F., Scimeca, J.C., Vandenbos, F., Michiels, J.F., Daculsi, G., Boileau, P., Weiss, P., Carle, G.F., and Rochet, N. Ectopic bone formation using an injectable biphasic calcium phosphate/Si-HPMC hydrogel composite loaded with undifferentiated bone marrow stromal cells. *Biomaterials* **27**, 3256, 2006.
23. van Gaalen, S.M., Dhert, W.J.A., van den Muysenberg, A., Oner, F.C., van Blitterswijk, C., Verbout, A.J., and de Bruijn, J.D. Bone tissue engineering for spine fusion: an experimental study on ectopic and orthotopic implants in rats. *Tissue Eng* **10**, 231, 2004.
24. Kim, H., Suh, H., Jo, S.A., Kim, H.W., Lee, J.M., Kim, E.H., Reinwald, Y., Park, S.H., Min, B.H., and Jo, I. *In vivo* bone formation by human marrow stromal cells in biodegradable scaffolds that release dexamethasone and ascorbate-2-phosphate. *Biochem Biophys Res Commun* **332**, 1053, 2005.
25. Krebsbach, P.H., Kuznetsov, S.A., Satomura, K., Emmons, R.V.B., Rowe, D.W., and Robey, P.G. Bone formation *in vivo*: comparison of osteogenesis by transplanted mouse and human marrow stromal fibroblasts. *Transplantation* **63**, 1059, 1997.
26. Musgrave, D.S., Bosch, P., Lee, J.Y., Pelinkovic, D., Ghivizzani, S.C., Whalen, J., Niyibizi, C., and Huard, J. *Ex vivo* gene therapy to produce bone using different cell types. *Clin Orthop Relat Res* **378**, 290, 2000.
27. Kojima, K., Bonassar, L.J., Ignatz, R.A., Syed, K., Cortiella, J., and Vacanti, C.A. Comparison of tracheal and nasal chondrocytes for tissue engineering of the trachea. *Ann Thorac Surg* **76**, 1884, 2003.
28. van Susante, J.L., Buma, P., Homminga, G.N., van den Berg, W.B., and Veth, R.P. Chondrocyte-seeded hydroxyapatite for repair of large articular cartilage defects: a pilot study in the goat. *Biomaterials* **19**, 2367, 1998.
29. Lu, J.X., Prudhommeaux, F., Meunier, A., Sedel, L., and Guillemain, G. Effects of chitosan on rat knee cartilages. *Biomaterials* **20**, 1937, 1999.
30. Dorotka, R., Windberger, U., Macfelda, K., Bindreiter, U., Toma, C., and Nehrner, S. Repair of articular cartilage defects treated by microfracture and a three-dimensional collagen matrix. *Biomaterials* **26**, 3617, 2005.
31. Marijnissen, W.J.C.M., van Osch, G.J.V.M., Aigner, J., Verwoerd-Verhoef, H.L., and Verhaar, J.A.N. Tissue-engineered cartilage using serially passaged articular chondrocytes. Chondrocytes in alginate, combined *in vivo* with a synthetic (E210) or biologic biodegradable carrier (DBM). *Biomaterials* **21**, 571, 2000.
32. Case, N.D., Duty, A.O., Ratcliffe, A., Muller, R., and Goldberg, R.E. Bone formation on tissue-engineered cartilage constructs *in vivo*: effects of chondrocyte viability and mechanical loading. *Tissue Eng* **9**, 587, 2003.

33. Cancedda, R., Cancedda, F.D., and Castagnola, P. Chondrocyte differentiation. *Int Rev Cytol* **159**, 265, 1995.
34. Hunziker, E.B. Mechanism of longitudinal bone-growth and its regulation by growth-plate chondrocytes. *Microsc Res Tech* **28**, 505, 1994.
35. Kirsch, T., Nah, H.D., Shapiro, I.M., and Pacifici, M. Regulated production of mineralization-competent matrix vesicles in hypertrophic chondrocytes. *J Cell Biol* **137**, 1149, 1997.
36. Anderson, H.C. Molecular-biology of matrix vesicles. *Clin Orthop Relat Res* **314**, 266, 1995.
37. Yaylaoglu, M.B., Yildiz, C., Korkusuz, F., and Hasirci, V. A novel osteochondral implant. *Biomaterials* **20**, 1513, 1999.
38. Garimella, R., Bi, X.H., Camacho, N., Sipe, J.B., and Anderson, H.C. Primary culture of rat growth plate chondrocytes: an *in vitro* model of growth plate histotype, matrix vesicle biogenesis and mineralization. *Bone* **34**, 961, 2004.
39. Boskey, A., and Camacho, N.P. FT-IR imaging of native and tissue-engineered bone and cartilage. *Biomaterials* **28**, 2465, 2007.
40. Jikko, A., Aoba, T., Murakami, H., Takano, Y., Iwamoto, M., and Kato, Y. Characterization of the mineralization process in cultures of rabbit growth plate chondrocytes. *Dev Biol* **156**, 372, 1993.
41. Cadet, E.R., Gafni, R.I., McCarthy, E.F., McCray, D.R., Bacher, J.D., Barnes, K.M. and Baron, J. Mechanisms responsible for longitudinal growth of the cortex: coalescence of trabecular bone into cortical bone. *J Bone Joint Surg Am* **85A**, 1739, 2003.
42. Lee, C., Grad, S., Wimmer, M., and Alini, M. The influence of mechanical stimuli on articular cartilage tissue engineering. *Cartilage Tissue Eng* **2**, 1, 2006.
43. Treczick, B., Lienau, J., Schell, H., Epari, D.R., Thompson, M.S., Hoffmann, J.E., Kadow-Romacker, A., Mundlos, S., and Duda, G.N. Endochondral ossification *in vitro* is influenced by mechanical bending. *Bone* **40**, 597, 2007.
44. Tanck, E., Hannink, G., Ruimerman, R., Buma, P., Burger, E.H., and Huiskes, R. Cortical bone development under the growth plate is regulated by mechanical load transfer. *J Anat* **208**, 73, 2006.
45. Dong, J., Uemura, T., Kojima, H., Kikuchi, M., Tanaka, J., and Tateishi, T. Application of low-pressure system to sustain *in vivo* bone formation in osteoblast/porous hydroxyapatite composite. *DJNL* **17**, 37, 2001.
46. Stevens, M., Marini, R., Schaefer, D., Aronson, J., Langer, R., and Shastri, V. *In vivo* engineering of organs: the bone bio-reactor. *Proc Natl Acad Sci USA* **102**, 11450, 2005.
47. Rinaudo, M. Chitin and chitosan: properties and applications. *Prog Polym Sci* **31**, 603, 2006.

Address reprint requests to:

Cristina Teixeira, D.M.D., M.S., Ph.D.

Department of Basic Science and Craniofacial Biology

and Department of Orthodontics

College of Dentistry

New York University

345 East. 24th St.

New York, NY 10010

E-mail: ct40@nyu.edu

Received: January 23, 2008

Accepted: June 10, 2008

Online Publication Date: August 28, 2008

